EClinicalMedicine 37 (2021) 100982

Contents lists available at ScienceDirect

EClinicalMedicine

journal homepage: www.elsevier.com/locate/eclinm

Research Paper

# $^{18}$F-florbetapir PET/MRI for quantitatively monitoring myelin loss and recovery in patients with multiple sclerosis: A longitudinal study

Min Zhang[a,†], You Ni[b,†], Qinming Zhou[b,†], Lu He[b], Huanyu Meng[b], Yining Gao[b], Xinyun Huang[a], Hongping Meng[a], Peihan Li[c], Meidi Chen[c], Danni Wang[d], Jingyi Hu[d], Qiu Huang[a,c], Yao Li[a,d], Fabien Chauveau[e], Biao Li[a,*], Sheng Chen[b,*]

[a] Department of Nuclear Medicine, Ruijin Hospital, Shanghai Jiao Tong University School of Medicine, Shanghai, China
[b] Department of Neurology, Ruijin Hospital, Shanghai Jiao Tong University School of Medicine, 197 Ruijin 2nd Road, Shanghai 200025, China
[c] School of Biomedical Engineering, Shanghai Jiao Tong University, Shanghai, China
[d] Institute for Medical Imaging Technology, School of Biomedical Engineering, Shanghai Jiao Tong University, Shanghai, China
[e] Univ Lyon, Lyon Neuroscience research Center, CNRS UMR5292, INSERM U1028, Univ Lyon 1, Lyon, France

ARTICLE INFO

*Article history:*
Received 26 November 2020
Revised 19 May 2021
Accepted 2 June 2021

*Keywords:*
$^{18}$F-florbetapir
PET/MRI
Demyelination
Myelin loss and recovery
Multiple sclerosis

ABSTRACT

*Background:* Amyloid positron emission tomography (PET) can measure in-vivo demyelination in patients with multiple sclerosis (MS). However, the value of $^{18}$F-labeled amyloid PET tracer, $^{18}$F-florbetapir in the longitudinal study for monitoring myelin loss and recovery has not been confirmed.

*Methods:* From March 2019 to September 2020, twenty-three patients with MS and nine healthy controls (HCs) underwent a hybrid PET/MRI at baseline and expanded disability status scale (EDSS) assessment, and eight of 23 patients further underwent follow-up PET/MRI. The distribution volume ratio (DVR) and standard uptake value ratio (SUVR) of $^{18}$F-florbetapir in damaged white matter (DWM) and normal-appearance white matter (NAWM) were obtained from dynamic and static PET acquisition. Diffusion tensor imaging-derived parameters were also calculated. Data were expressed as mean ± standard deviation with 99% confidence interval (99%CI).

*Finding:* The mean DVR (1.08 ± 0.12, 99%CI [1.02 ~ 1.14]) but not the mean SUVR of DWM lesions was lower than that of NAWM in patients with MS (1.25 ± 0.10, 99%CI [1.20 ~ 1.31]) and HCs (1.29 ± 0.08, 99%CI [1.23 ~ 1.36]). A trend toward lower mean fractional anisotropy (374.95 ± 45.30 vs. 419.07 ± 4.83) and higher mean radial diffusivity (0.45 ± 0.05 vs. 0.40 ± 0.01) of NAWM in patients with MS than those in HCs was found. DVR decreased in DWM lesions with higher MD (rho = -0.261, 99%CI [-0.362 ~ -0.144]), higher AD (rho = -0.200, 99%CI [-0.318 ~ -0.070]) and higher RD (rho = -0.198, 99%CI [-0.313 ~ -0.075]). Patients' EDSS scores were reduced ($B$ = 0.04, 99%CI [-0.005 ~ 0.084]) with decreased index of global demyelination in the longitudinal study.

*Interpretation:* Our exploratory study suggests that dynamic $^{18}$F-florbetapir PET/MRI may be a very promising tool for quantitatively monitoring myelin loss and recovery in patients with MS.

*Funding:* Shanghai Pujiang Program, Shanghai Municipal Key Clinical Specialty, Shanghai Shuguang Plan Project, Shanghai Health and Family Planning Commission Research Project, Clinical Research Plan of SHDC, French-Chinese program "Xu Guangqi".





**Evidence before this study**

The research on in vivo monitoring of myelin loss and recovery in patients with multiple sclerosis (MS) using amyloid

* Corresponding authors.
*E-mail addresses:* lb10363@rjh.com.cn (B. Li), mztcs@163.com (S. Chen).
† Min Zhang, You Ni and Qinming Zhou contributed equally to this work.

https://doi.org/10.1016/j.eclinm.2021.100982

positron emission tomography (PET) has increased in recent years. The research teams from the US and Europe have conducted clinical trials of $^{11}$C-PiB or $^{18}$F-labelled amyloid PET tracers for the diagnosis of MS. Compared with $^{11}$C-PiB, the $^{18}$F-labelled amyloid tracer such as $^{18}$F-florbetapir has higher binding of white matter and longer half-life for better clinical practice. However, a longitudinal study of $^{18}$F-florbetapir PET for monitoring myelin content change has not been performed in previous studies.

**Added value of this study**

This is an exploratory longitudinal study of hybrid $^{18}$F-florbetapir PET/magnetic resonance imaging (MRI) in Chinese patients with MS. We demonstrate that dynamic $^{18}$F-florbetapir PET may be a very promising tool for quantitatively monitoring myelin loss and recovery in patients with MS, and well correlates with changes in patients' expanded disability status scale (EDSS). Moreover, diffusion tensor imaging (DTI) may synchronously provide information on microstructure changes of damaged white matter (DWM) and normal-appearance white matter (NAWM) in patients with MS.

**Implications of all the available evidence**

This study suggests that hybrid $^{18}$F-florbetapir PET/MRI will become a powerful technique for monitoring the progress of MS and evaluating the efficacy of remyelination-targeted drugs in the future.

## 1. Introduction

Multiple sclerosis (MS) is an inflammatory demyelinating disease of the central nervous system (CNS) that commonly causes neurological disability in young adults and places a heavy burden on patients' families in China [1, 2]. Therefore, the International Multiple Sclerosis Alliance has established World MS Day since May 27, 2009, to promote related research and medical development. In recent years, preclinical studies have suggested that drugs that promote remyelination (miconazole, clobetasol, benztropine, opicinumab, etc.) can better reduce the incidence of long-term disability [3-6] compared with conventional anti-inflammatory therapy. However, one of the challenges of the clinical translation of these drugs is the urgent need for a reliable quantitative assessment of myelin content, and there is currently no consensus on which technique should be used.

Currently, MS imaging diagnosis mainly relies on conventional magnetic resonance imaging (MRI). As commonly used anatomical imaging (T1WI, T2WI) signals are affected by many factors, such as inflammation, blood-brain barrier permeability, edema, demyelination, and axonal injury, it is difficult to distinguish and quantify the pathological changes of myelin loss and recovery. Thus, its correlation with long-term prognosis is not well established. Advanced MRI sequences, including diffusion tensor imaging (DTI), magnetization transfer imaging (MTI), and myelin water imaging (MWF), are gaining increasing attention as they may provide enhanced specificity to myelin [7]. DTI can quantitatively evaluate the diffusion movement of water in the tissue and is becoming a promising imaging technique that reflects the changes in the microstructure of the white matter (WM) tract. The DTI-derived radial diffusivity (RD) value increases with the loss of myelin, and the increase in axial diffusivity (AD) is related to axonal injury [8], but these parameters are also sensitive to inflammation. The latest developments of MWF (mcDESPOT [9]) and MTI (ihMT [10]) may provide more effective methods to quantify the myelin content but await preclinical validation and clinical standardization. However, the above sequences based on the principle of water diffusion anisotropy or the combination of water and lipids still indirectly reflect the content of the myelin sheath. Therefore, although advanced MRI provides important information on the microstructure changes of MS lesions, there is still a lack of effective imaging tools for directly quantifying myelin content.

Positron emission tomography (PET) is a noninvasive molecular imaging technique that can quantitatively monitor biochemical or physiological processes and can provide more direct monitoring of myelin content. Pioneering work by the group of Stankoff B et al. proved that the amyloid PET tracer $^{11}$C-PiB originally developed for the diagnosis of Alzheimer's disease has the ability to image myelin, which can be used to quantify myelin loss and recovery in patents with MS and is related to patient disability [11-14]. The binding of amyloid tracer to WM is due to the $\beta$-sheet-like structure of myelin base protein (MBP) similar to amyloid plaques [15], making PET imaging with amyloid tracer a new method for myelin imaging. Other independent research teams further confirmed the ability of $^{11}$C-PiB PET to detect focal demyelination under different pathological conditions [16-18]. However, because the half-life of $^{11}$C is very short (only 20.5 min), the clinical application of $^{11}$C-PiB is severely limited. Therefore, second-generation $^{18}$F (approximately 110 min)-labeled tracers with higher WM binding rates need to be developed. A recent study has shown that $^{18}$F-labeled amyloid tracers such as $^{18}$F-florbetapir and $^{18}$F-florbetaben have higher binding of WM than $^{11}$C-PiB [19], and a few research teams, including our team, have carried out myelin PET imaging using $^{18}$F-florbetapir [20-22] and $^{18}$F-florbetaben [23, 24] for clinical practice. Although a pioneering longitudinal study using $^{11}$C-PiB from Bodini B, et al. [12] has indicated the effectiveness of amyloid PET for monitoring demyelination and remyelination, longitudinal study of $^{18}$F-florbetapir PET for monitoring myelin content change has not been performed in previous researches with limited evidence about the amyloid tracers.

In this study, we performed hybrid $^{18}$F-florbetapir PET/MRI scans at baseline and during the follow-up period to quantitatively assess myelin loss and recovery in patients with MS, and then analyzed the correlation between $^{18}$F-florbetapir uptake and DTI measurements as well as the clinical disease score.

## 2. Materials and methods

### 2.1. Subjects

Twenty-three patients (12 males and 11 females, average age 41.4 $\pm$ 15.0 years) with a definite diagnosis of relapsing-remitting MS (RRMS) according to the 2017 revised McDonalds criteria [25] and nine healthy controls (HCs, 4 males and 5 females, average age 38.3 $\pm$ 13.4 years) were recruited in the study from March 2019 to September 2020. The inclusion and exclusion criteria for MS patients and HCs were listed in Supplemental Table 1. All patients underwent clinical assessments, including clinical disability through the expanded disability status scale (EDSS) before PET/MRI scan at baseline. The clinical characteristics of the enrolled patients with MS and HCs are summarized in Table 1 and listed in detail in Supplemental Table 2. Eight of 23 patients underwent not only the baseline scan but also the follow-up scan, which occurred an average of 194 $\pm$ 61 days after the baseline scan (Supplemental Table 5). Their EDSS scores at the follow-up scan were also evaluated, and then EDSS difference ($\delta$ EDSS), defined as the follow-up score minus the baseline score, was calculated.

All procedures performed in the study involving human participants were conducted in accordance with the principles of the Declaration of Helsinki and national regulations. The study was approved by the Ethics Committee of Ruijin Hospital, Shanghai Jiao

**Table 1**
Patients with MS and HCs' characteristics.

| | Patients with MS | HCs |
|---|---|---|
| Number | 23 | 9 |
| Gender (male/female) | 12/11 | 4/5 |
| Age (year) | 41.4 ± 15.0 (32.6 - 50.3) | 38.3 ± 13.4 (23.3 - 53.3) |
| Disease Course | RRMS | / |
| Treatment at study entry (%) | | |
| No treatment | 47.8% | / |
| Methylprednisolone | 47.8% | / |
| Teriflunomide | 4.4% | / |
| EDSS at baseline | 2.6 ± 1.6 (1.6 - 3.5) | / |
| Disease duration (month) | 54.1 ± 45.7 (27.2 - 81.0) | / |
| Annualized relapse rate | 0.5 ± 0.2 (0.3 - 0.6) | / |

Data were expressed as mean ± standard deviation with 99% confidence interval (99%CI).

Tong University School of Medicine. All the patients provided written informed consent. The manuscript adhered strictly to STROBE guidelines.

### 2.2. PET/MRI acquisition

A hybrid PET/MRI scan was performed with a Biograph mMR system (Siemens, Erlangen, Germany) with a NEMA PET resolution of 4.2 mm. After intravenous injection of 287.9 ± 19.4 MBq of $^{18}$F-florbetapir, dynamic PET acquisition in list mode over 60 min was started immediately. During PET acquisition, a 3D T1 magnetization-prepared rapid acquisition gradient echo (T1 MPRAGE, Repetition Time 1900 ms; Echo Time 2.44 ms; voxel size: 0.5 × 0.5 × 1.0 mm), a 3D T2-weighted fluid-attenuated inversion recovery (T2 FLAIR, Repetition Time 5000 ms; Echo Time 385 ms; voxel size: 0.5 × 0.5 × 0.9 mm), and a diffusion tensor echo-planar imaging sequence (DTI, Repetition Time 5400 ms; Echo Time 95 ms; voxel size: 1.7 × 1.7 × 4.0 mm) were acquired. The PET image was reconstructed by a point spread function algorithm with 344 × 344 pixels, 4 iterations, 21 subsets and a filter with a full width at half maximum of 2 mm.

### 2.3. Image data analysis

Image standardization and segmentation were performed using statistical parametric mapping software (SPM12, Wellcome centre for Human Neuroimaging, University College London, UK). Both PET and MRI images were first normalized to MNI152 space by SPM12. The lesion prediction algorithm in the Lesion Segmentation Tool (LST) toolbox was used for damaged white matter (DWM) lesion segmentation. The choroid part that was incorrectly segmented as the lesion was removed. Each individual lesion was segmented with the connected component labeling function "bwlablen (mask, 18)" from MATLAB software (The MathWorks, Inc., USA), and lesions with less than 8 voxels on T2 FLAIR images were removed according to Egger C et al. [26]. The total volume of all T2 lesions as an indicator of macroscopic DWM lesion load was calculated. Total WM, gray matter (GM) and cerebrospinal fluid (CSF) were automatically segmented using SPM12 software. Additionally, to reduce potential bias from partial volume effects on PET images, lesions smaller than the NEMA PET resolution (axial diameter < 4.2 mm) were not considered in our study, and an image erosion operation on the normal WM template (indented by one pixel) around the CSF was performed. Normal-appearing white matter (NAWM) in patients with MS was derived by subtracting the DWM segmentation from the total WM segmentation (Fig. 1b). PET images were coregistered to individual volumetric T2 FLAIR images using Siemens molecular imaging neurology software on the syngovia client server.

To avoid blood sampling in our patient cohort, we chose to quantify our dynamic PET scans using a reference region approach. According to the supervised clustering method already validated for the extraction of the reference region time activity curve of $^{11}$C-PiB [12, 13] or $^{18}$F-florbetapir [22], normal GM was selected as a reference region. The Logan graphical reference method [27] was then applied at the voxel level on PET scans to produce a parametric map of $^{18}$F-florbetapir binding measured as the distribution volume ratio (DVR, defined as the ratio of the total distribution volume between the target and the reference region). Static $^{18}$F-florbetapir PET image was quantified using the standardized uptake value 40–60 min after injection ($SUV_{40-60}$), which was defined with respect to activity per unit volume (C, kBq/ml) in the volume of interest (VOI), body weight (BW, kg), and injected dose (ID; MBq); SUV=$C$/(ID/BW). The cerebellar cortex was used as the reference region for the standardized uptake value relative ratios (SUVRs). The index of global demyelination for each patient was defined as the total T2 lesion load in mm$^3$ multiplied by the mean DVR. The change rate of the index of global demyelination ($\delta$ global demyelination) was then defined as the percentage change in the index of global demyelination at follow-up from that at baseline for assessing myelin recovery.

Diffusion tensor images (DTIs) were first eddy-current corrected and head-motion corrected by the FMRIB Diffusion Toolbox (FSL, https://fsl.fmrib.ox.ac.uk/fsl/fslwiki/FSL) for each subject. The corrected images were then tensor fitted to acquire the fractional anisotropy (FA), mean diffusivity (MD), axial diffusivity (AD) and radial diffusivity (RD), which were expressed as the original value × 1000. Subsequently, we linearly registered the b0 map to the individual T1-weighted map and normalized the T1-weighted map to MNI152 space by SPM12. The deformable map and the transformation matrix obtained from the previous steps were applied to the four diffusion maps.

### 2.4. Statistical analysis

All statistical analyses were performed using SPSS 20.0 (IBM Corp., Armonk, NY, USA) and GraphPad PRISM 7.0 (GraphPad Software, La Jolla, CA, USA). Data were expressed as mean ± standard deviation with 99% confidence interval (99%CI). The relationships between the $^{18}$F-florbetapir DVR and MRI measurements and SUVR on all lesions were initially analyzed using the Spearman correlation as data did not conform to a Gaussian distribution. The relationship between the change rate of global demyelination and the EDSS difference was evaluated using a multifactor linear regression method taking into account the factors of patients' age, interval days between the baseline and follow-up scans and whether to be treated during the interval. The coefficients obtained from Spearman correlation (rho) and multifactor linear regression (B) were expressed as mean coefficients with 99%CI. Bootstrapping method using 1000 repeated sampling was applied in our study with non-random and smaller sample.

### 2.5. Role of the funding sources

The funding sources provided the financial support. They had no role in the study design, collection, analysis and interpretation of the data, writing of the manuscript, or decision to submit the paper for publication. All authors had full access to the full data in the study and accept responsibility to submit for publication.

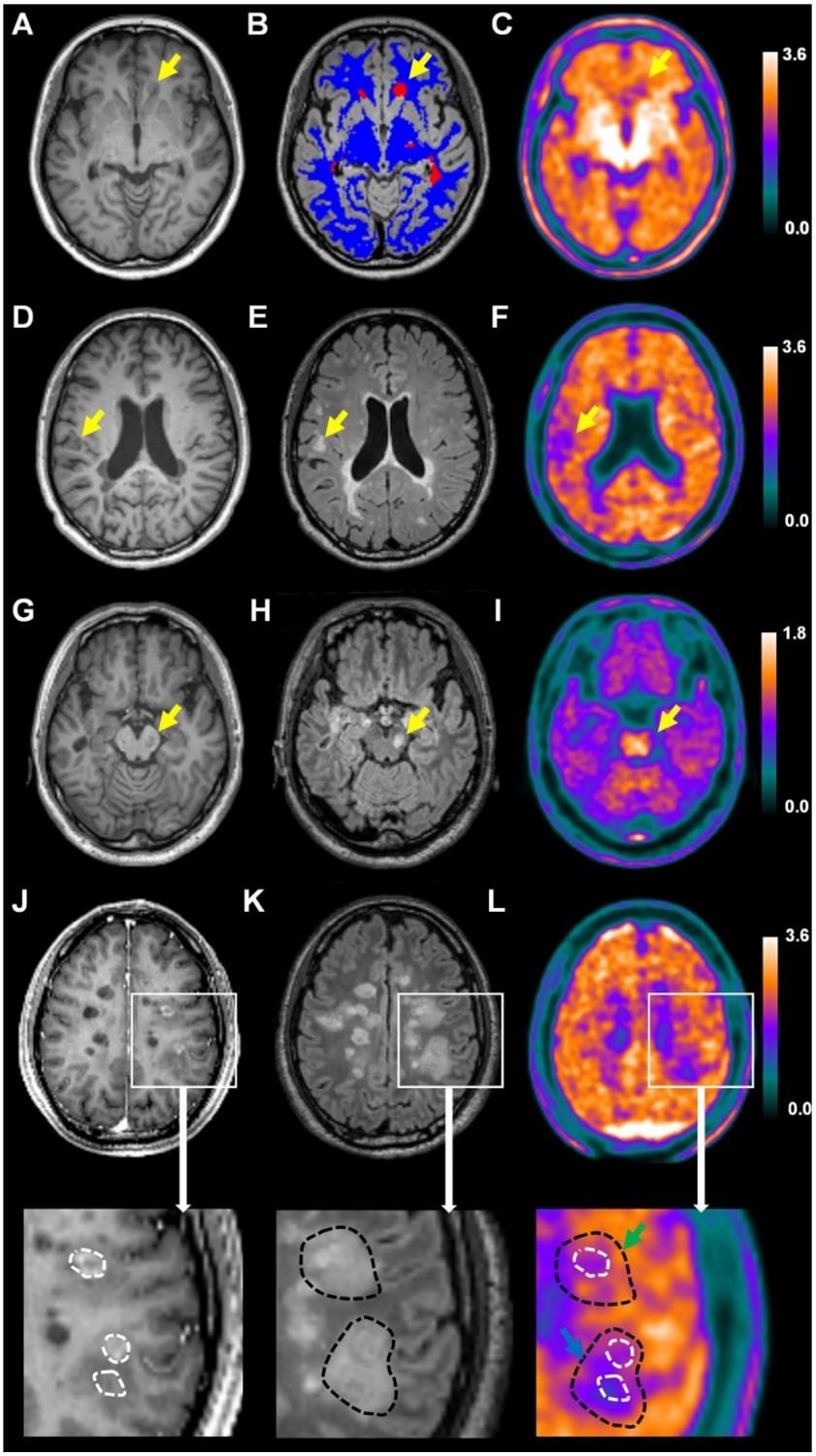


**Fig. 1.** Representative PET/MRI images from the patients No. 2 (A-C), No. 5 (D-F) and No. 23 (G-L) at baseline scan. (A, D, G) Typical DWM lesions with T1-weighted hypointensity and (B, E, H) T2-weighted FLAIR hyperintensity next to the lateral, under the cerebral cortex, and brainstem (yellow arrow); (B) NAWM (blue) and DWM (red) segmentation on T2-weighted FLAIR MRI; (C, F, I) $^{18}$F-florbetpir DVR parametric map showed decreased $^{18}$F-florbetapir uptake (yellow arrow) in DWM lesions; (J) In the patient No.23, gadolinium contrast-enhanced T1-weighted MRI showed the edge enhancement of some acute demyelinating lesions (white dotted lines), accompanied by surrounding edema zone with slightly lower signal intensity, indicating a disease activity; (K) T2 hyperintensity was found in both demyelinating lesions and surrounding edema zone (black dotted lines); (L) Reduced $^{18}$F-florbetpir DVR was obviously observed in the contrast-enhanced lesions (white dotted lines). However, $^{18}$F-florbetpir DVR in the edema zone (range between white and black dotted lines) was found to be similar to (green arrow) or lower than NAWM (blue arrow), suggesting that varying degrees of demyelination occurred in the neuroinflammatory zone. DVR: distribution volume ratio; DWM: damaged white matter; MRI: magnetic resonance imaging; NAWM: normal-appearing white matter; PET/MRI: positron emission tomography/magnetic resonance imaging.

## 3. Results

### 3.1. PET/MRI measurements of DWM and NAWM in patients with MS and HCs

Detailed PET/MRI measurements of DWM and NAWM for each patient with MS and HC are listed in Supplemental Table 3. From the patient-based analysis in Table 2, lower mean DVRs were found in DWM (1.08 ± 0.12, 99%CI [1.02 ~ 1.14]) compared to NAWM in patients with MS (1.25 ± 0.10, 99%CI [1.20 ~ 1.31]) and HCs (1.29 ± 0.08, 99%CI [1.23 ~ 1.36]). Fig. 1A-1L shows decreased $^{18}$F-florbetapir binding in typical MS lesions with T1 hypointensity and T2 hyperintensity. In addition, the $^{18}$F-florbetapir DVR of the edema zone around contrast-enhanced lesions was found to be similar to or lower than NAWM in the acute phase of MS (Fig. 1J-1L), suggesting that varying degrees of demyelination might occur in the neuroinflammatory zone.

However, the mean SUVR showed no difference between DWM (1.44 ± 0.21, 99%CI [1.33 ~ 1.55]) and NAWM in patients with MS (1.42 ± 0.18, 99%CI [1.32 ~ 1.51]) or HCs (1.55 ± 0.14, 99%CI [1.43 ~ 1.66]). Except for FA, the mean MD, AD and RD were higher in DWM of patients with MS than in NAWM of patients with MS and HCs, as shown in Table 2. There was no difference in mean DVR or mean SUVR between NAWM in patients with MS and HCs. Additionally, a trend toward lower mean FA and higher mean RD of NAWM in patients with MS was found when compared with NAWM in HCs.

$^{18}$F-florbetapir DVR and SUVR are calculated through dynamic and static PET acquisition, respectively. We compared the differences in these two parameters between DWM lesions with different axial diameters [< 5 mm ($n$ = 21), 5–10 mm ($n$ = 23), 10–15 mm ($n$ = 20), >15 mm ($n$ = 22)] and NAWM in patients with MS and HCs (Fig. 2A and 2B). The mean DVRs of DWM lesions in the four diameter ranges were lower than that of NAWM in HCs and patients with MS, except that there was no difference of mean DVRs between DWM lesion with < 5 mm axial diameter and NAWM in patients with MS. A trend toward larger DWM lesions with lower SUVR was found when compared with NAWM in patients with MS and HCs. Representative PET/MRI images with various lesion sizes (Fig. 2C-2E) showed that the reduction in $^{18}$F-florbetapir uptake was obviously observed on both the DVR parametric map and SUV map for T2 lesions with larger axial diameters, but for T2 lesions with smaller axial diameters, a visible difference in $^{18}$F-florbetapir uptake between DWM lesions and NAWM could only be distinguished on the DVR parametric map.

In this study, 16 of total 23 patients with MS had performed CE-MRI one week before or after PET/MRI at baseline. Total 25 gadolinium-enhanced (Gd+) lesions were observed in 5 of 16 patients with CE-MRI (Supplemental Table 2). We compared the mean DVR between enhanced or non-enhanced lesions and NAWM in the five patients (Supplemental Fig. 1). Both Gd+ (1.10 ± 0.07, 99%CI [1.04 ~ 1.17]) and Gd- lesions (1.06 ± 0.05, 99%CI [1.01 ~ 1.10]) showed lower mean DVR than that of NAWM (1.20 ± 0.06, 99%CI [1.18 ~ 1.26]).

The mean $^{18}$F-florbetapir DVR, SUVR, FA, MD, AD, RD, and T2 load of DWM lesions were not related to EDSS in patients with MS at the baseline scan (Supplemental Table 4).

### 3.2. Relationship between $^{18}$F-florbetapir DVR and DTI-derived parameters or SUVR

From a lesion-based approach (Fig. 3A-3E), $^{18}$F-florbetapir DVR decreased in DWM lesions with a higher MD (rho = −0.261, 99%CI [−0.362 ~ −0.144]), AD (rho = −0.200, 99%CI [−0.318 ~ −0.070]) and RD (rho = −0.198, 99%CI [−0.313 ~ −0.075]). DVR showed no correlation with FA (rho = 0.061, 99%CI [−0.053 ~ 0.181]) in DWM

**Table 2**
PET/MRI quantitative parameters of all patients with MS and HCs.

| | Patients with MS | | | HCs | |
|---|---|---|---|---|---|
| | DWM | NAWM | Ratio[1] | NAWM | Ratio[2] |
| PET/MRI measurements | | | | | |
| mean DVR | 1.08 ± 0.12 (1.02 - 1.14) | 1.25 ± 0.10 (1.20 - 1.31) | 0.87 ± 0.02 (0.82 - 0.91) | 1.29 ± 0.08 (1.23 - 1.36) | 0.97 ± 0.03 (0.89 - 1.04) |
| mean SUVR | 1.44 ± 0.21 (1.33 - 1.55) | 1.42 ± 0.18 (1.32 - 1.51) | 1.01 ± 0.02 (0.96 - 1.06) | 1.55 ± 0.14 (1.43 - 1.66) | 0.97 ± 0.04 (0.86 - 1.09) |
| T2 lesion load (mm$^3$) | 23,270.91 ± 21,954.31 (10,367.24 - 36,174.60) | / | / | / | / |
| mean FA | 395.40 ± 57.95 (360.64 - 425.85) | 374.95 ± 45.30 (345.26 - 395.57) | 1.06 ± 0.02 (0.99 - 1.12) | 419.07 ± 4.83 (414.89 - 422.36) | 0.91 ± 0.03 (0.83 - 0.97) |
| mean MD | 0.65 ± 0.05 (0.62 - 0.67) | 0.57 ± 0.04 (0.55 - 0.60) | 1.13 ± 0.02 (1.09 - 1.17) | 0.54 ± 0.01 (0.53 - 0.54) | 1.05 ± 0.02 (1.02 - 1.09) |
| mean AD | 0.93 ± 0.06 (0.90 - 0.96) | 0.81 ± 0.03 (0.80 - 0.83) | 1.14 ± 0.02 (1.10 - 1.18) | 0.80 ± 0.01 (0.79 - 0.81) | 1.01 ± 0.01 (0.98 - 1.05) |
| mean RD | 0.50 ± 0.05 (0.47 - 0.54) | 0.45 ± 0.05 (0.43 - 0.48) | 1.13 ± 0.02 (1.07 - 1.18) | 0.40 ± 0.01 (0.40 - 0.41) | 1.09 ± 0.02 (1.04 - 1.15) |

DTI-derived parameters were expressed as original value × 1000.
Ratio[1] is the ratio of each quantitative image parameter between DWM and NAWM in patients with MS.
Ratio[2] is the ratio of each quantitative image parameter between NAWM in patients with MS and NAMW in HCs.
Data were expressed as mean ± standard deviation with 99% confidence interval (99%CI).

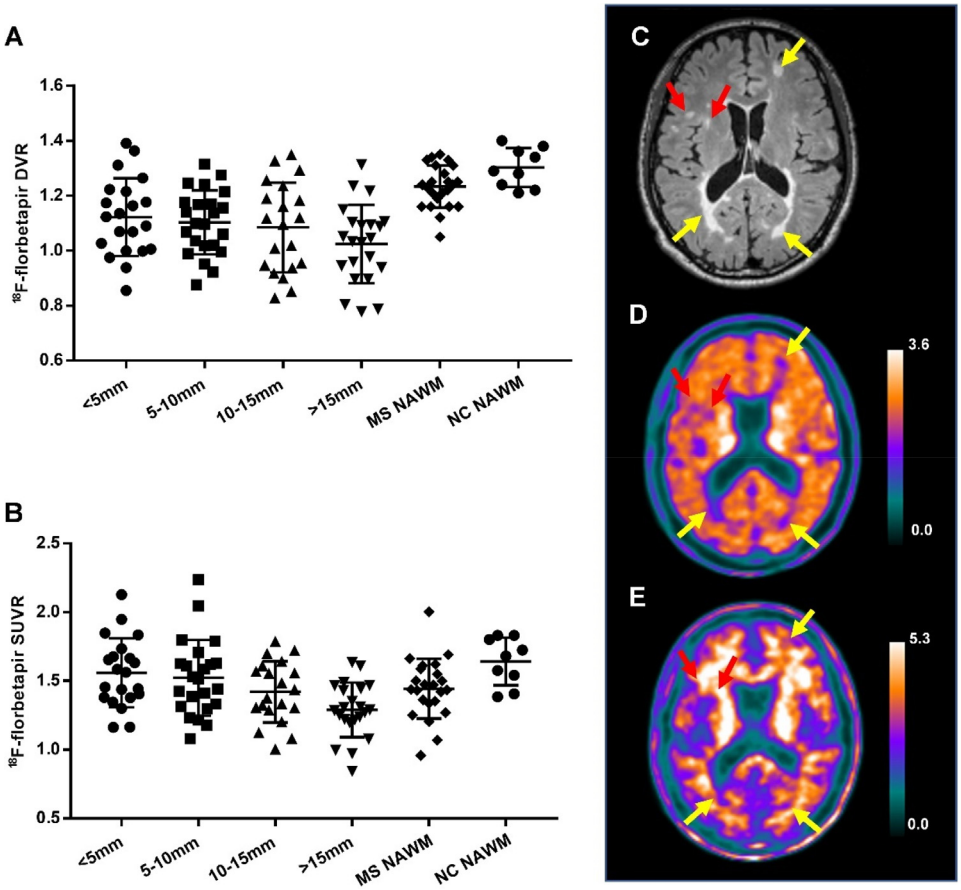


**Fig. 2.** Relationship between $^{18}$F-florbetapir uptake and size of DWM lesions (axial diameter < 5 mm, 5–10 mm, 10–15 mm, >15 mm). The three horizontal lines in each column of the data set indicated mean ± standard deviation. (A) mean $^{18}$F-florbetapir DVR and standard deviation in DWM lesions and NAWMs for MS patients and HCs. Mean DVRs of DWM lesions in the four diameter ranges were lower than that of NAWM in HCs, but only DWM lesions with 5–10 mm, 10–15 mm and >15 mm diameters showed lower mean DVRs than that of NAWM in patients with MS. (B) mean SUVR and standard deviation in DWM lesions and NAWMs for MS patients and HCs. Only DWM lesions with >15 mm diameter showed lower mean SUVR than that of NAWM in HCs. A trend toward lower mean SUVR with higher axial diameter of DWM lesions was found. Representative PET/MRI images with various lesion sizes on (C) T2 FLAIR MRI, (D) $^{18}$F-florbetapir DVR parametric map and (E) SUV map. For the T2 lesions with larger axial diameter (yellow arrow, 9.48, 38.09, 39.14 mm), visible reduction of $^{18}$F-florbetapir uptake were observed on both DVR parameter map and SUV map. However, for the T2 lesions with smaller axial diameter (red arrow, 4.74, 5.12 mm), there was no visible difference of $^{18}$F-florbetapir uptake between T2 lesions and surrounding NAWM on SUV map, whereas $^{18}$F-florbetapir DVR was still reduced on the same T2 lesions. DWM: damaged white matter; DVR: distribution volume ratio; HCs: healthy controls; NAWM: normal appearing white matter; PET/MRI: positron emission tomography/magnetic resonance imaging; SUVR: standardized uptake value ratio.

lesions. SUVR was positively correlated with DVR (rho = 0.675, 99%CI [0.606 ~ 0.740]).

### *3.3. Relationship between the change rate of global demyelination and the EDSS difference in the longitudinal study*

Eight of the total patients underwent both baseline and follow-up scans (Supplemental Table 5). Patients' EDSS scores were reduced ($B$ = 0.04, 99%CI [−0.005 ~ 0.084]) with a decrease in the index of global demyelination (Fig. 4). Representative T2 FLAIR MRI and $^{18}$F-florbetapir DVR maps (Fig. 5A-5L) showed that both focal areas of T2 hyperintensity and those of abnormally reduced $^{18}$F-florbetapir binding in DWM lesions decreased from baseline to follow-up, indicating that myelin recovery might occur after inflammation disappearance.

## 4. Discussion

Our exploratory longitudinal study demonstrates that $^{18}$F-florbetapir PET is a very promising tool that could quantitatively detect myelin loss and recovery in MS lesions. The DVR obtained by 60-min dynamic PET acquisition is less affected by lesion size for distinguishing DWM and NAWM than the static $SUVR_{40–60}$, and is suitable as a quantitative indicator for monitoring changes in the myelin content. Furthermore, MRI in the hybrid PET/MRI device not only aids in locating MS lesions on PET using conventional MRI sequences but also synchronously provides information on acute inflammation edema and DTI-based myelin microstructure changes in WM.

First, reduced $^{18}$F-florbetapir binding of focal DWM lesions in patients with MS could be observed when compared with those of NAWM in patients with MS and HCs. Different from T1-hypointensity and T2-hyperintensity signals reflecting indistinguishable inflammatory edema and demyelination [28, 29], $^{18}$F-florbetapir PET may be more specific than conventional MRI to quantify changes of myelin content in DWM lesions.

There are still two issues that need to be clarified before determining the advantages of amyloid PET for myelin imaging. One is quantitative measurement of myelin loss by amyloid PET in inflammatory edema. Neuroinflammation is an important pathological process in addition to demyelination in patients with MS. It has been reported that microglia are activated in MS lesions, and microglia-mediated inflammation is related to T2 hyperintensity and T2 lesion load [30]. As the biological substrate of PET signal change within inflammatory edema is not clear, the impact of increased permeability of the blood-brain barrier on PET quan-

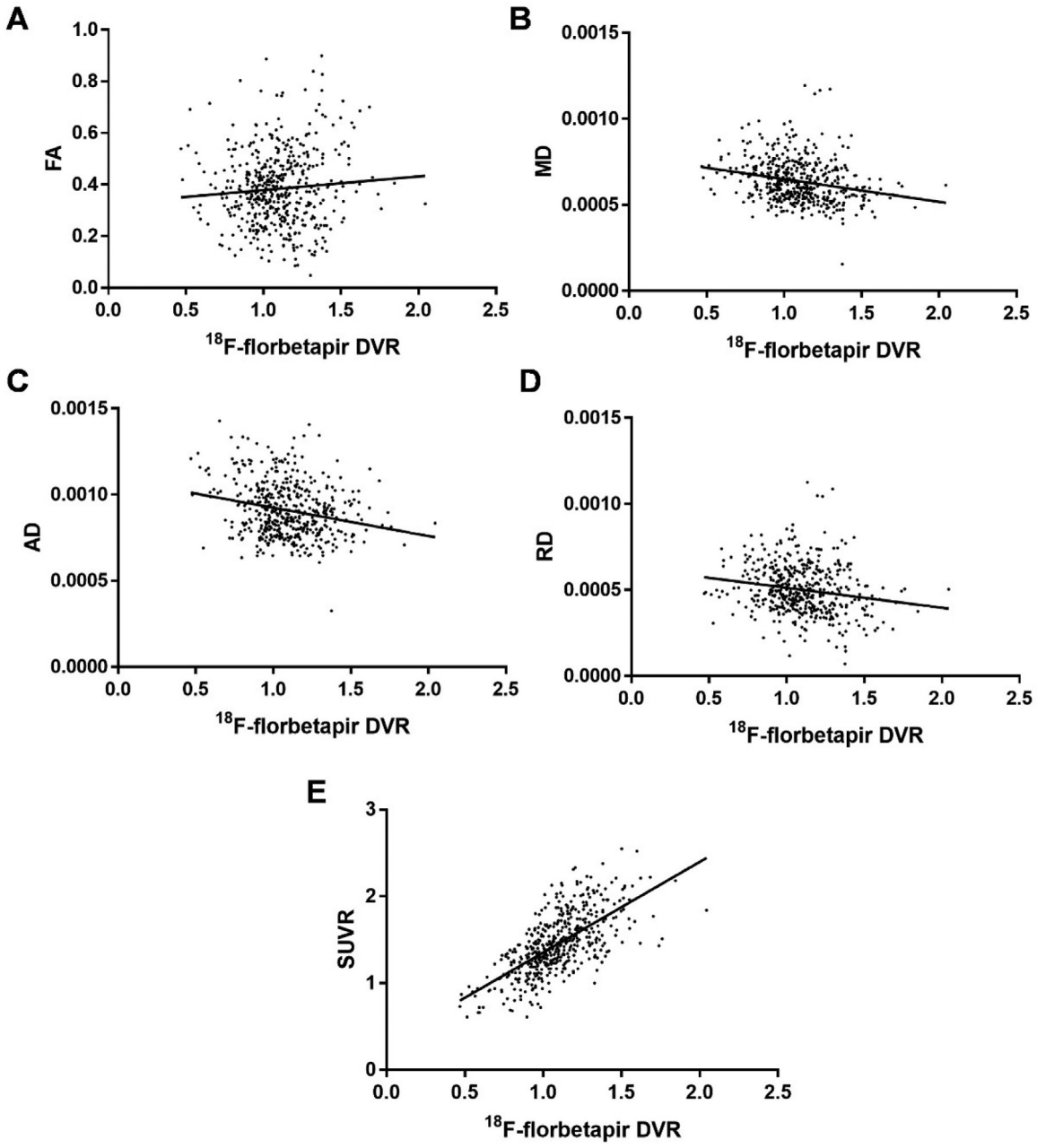


**Fig. 3.** Correlation between $^{18}$F-florbetapir DVR and DTI-derived (A) FA, (B) MD, (C) AD, (D) RD, (E) standardized uptake value ratio (SUVR) in DWM lesions for a lesion-based approach. DVR decreased in DWM lesions with higher MD (rho = −0.261, 99%CI [−0.362 ~ −0.144]), higher AD (rho = −0.200, 99%CI [−0.318 ~ −0.070]) and higher RD (rho = −0.198, 99%CI [−0.313 ~ −0.075]). DVR in DWM lesions showed no correlation with FA (rho = 0.061, 99%CI [−0.053 ~ 0.181]). SUVR was positively correlated with DVR (rho = 0.675, 99%CI [0.606 ~ 0.740]). AD: axial diffusivity; DTI: diffusion tensor imaging; DVR: distribution volume ratio; DWM: damaged white matter; FA: fractional anisotropy; MD: mean diffusivity; RD: radial diffusivity; SUVR: standardized uptake value relative ratio.

tification of lesions has been questioned. In our study, the average level of $^{18}$F-florbetapir binding in T2-defined lesions including edema zone (the part outside the Gd+ ring but still within T2-hyperintensity) was reduced, though its distribution in edema zone was obviously heterogeneous. Bodini B, et al. [12] suggested that the inflammatory component did not negatively bias the estimation of the myelin change because a moderate binding reduction of amyloid tracer was also observed in Gd+ inflammatory lesions. We speculated that the heterogeneity of tracer distribution in the edema zone may be due to a mixed pathological state of inflammatory cell infiltration and initial stage of demyelination in active MS plaque [31]. As the number of Gd+ lesions is small in our study, more strong evidences will be needed to identify this hypothesis.

The other is that decreased $^{18}$F-florbetapir binding may exist in NAWM around T2-defined lesions. Although the difference of mean $^{18}$F-florbetpir DVR in NAWM between patients with MS and HCs did not show difference in our study, the postmortem study by De Groot CJ et al. supported that, in addition to demyelination in T2 hyperintensity lesions in brain samples of patients with MS, the myelin density in NAWM around T2 lesions also decreased [28]. In effect, Bodini B, et al. [12] and Carotenuto A, et al. [22] have reported a decreased binding of amyloid tracer in the area 2 to 8 mm outside the edge of the T2 lesion, suggesting that the range

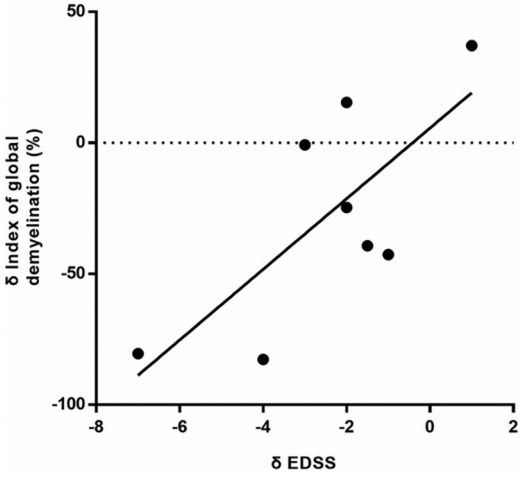


**Fig. 4.** The relationship between the change rate ($\delta$) of global demyelination and EDSS difference ($\delta$ EDSS) was evaluated using multi-factor linear regression method. Taking into account the factors of patients' age, interval days between the baseline and follow-up scans and whether to be treated during the interval, patients' EDSS reduced with the decrease of global demyelination ($B = 0.04$, 99%CI [−0.005 ~ 0.084]).

of demyelinating lesions reflected by amyloid PET might be larger than that defined by T2WI.

As the current researches of amyloid PET tracer for myelin imaging generally have small sample size, no strong conclusion that amyloid PET is superior to conventional MRI in detecting demyelination in terms of specificity and sensitivity could be drawn yet.

Second, EDSS and myelin changes were correlated in the longitudinal $^{18}$F-florbetapir PET study, suggesting that myelin recovery might contribute to the decrease in EDSS score. Previous [12, 22] and our present studies showed that EDSS was not related to $^{11}$C-PiB or $^{18}$F-florbetapir DVR in T2 lesions at baseline. Therefore, longitudinal amyloid PET reflecting the balance between the loss and recovery of myelin in patients with MS could better assess the development of clinical disease status of MS and disease-modifying treatments. Additionally, the disease status in patients with MS is related not only to myelin loss and recovery but also to axon injury as well as the involved brain region. $^{18}$F-florbetapir PET combined with the measurement of neuronal activity markers, such as N-acetyl aspartate through magnetic resonance spectroscopy [32], may further clarify the effect of demyelination, myelin recovery and axon loss on patients' disabilities. Hybrid PET/MRI device can simultaneously reveal the interaction between demyelination, myelin recovery, and axonal degeneration, providing a unique opportunity to evaluate these pathological processes in patients with MS.

Third, compared with dynamic PET, static PET requires less time for scanning. Meanwhile, the software accompanying the PET workstation can calculate the SUV without additional software processing, making clinical practice more convenient. Therefore, whether the ability of the SUVR based on static PET imaging for detecting demyelination was equivalent to dynamic DVR was evaluated in this study. However, although $^{18}$F-florbetapir SUVR was positively correlated with DVR, SUVR was not as effective as DVR in distinguishing DWM from NAWM. The smaller the DWM lesion (which means that it may be less demyelinated, with a smaller difference in $^{18}$F-florbetapir uptake between DWM and NAWM), the more difficult it is to distinguish between the two tissues. It should be noted that we performed a 60-min dynamic PET scan but not a 90-min scan, as in previous studies [22, 12]. One of the reasons is that the duration of 90 min is too long to be accepted by most patients. The second is that the time-activity curve of $^{18}$F-florbetapir in the WM almost reaches a plateau at 40–60 min (data not shown), and the dynamic 60-min scan already has good detection of MS lesions. Therefore, $SUVR_{40-60}$ could not replace DVR for reliably monitoring changes in myelin content. However, this conclusion may change if the scan time is extended to 90 min, with a static scan between 70 and 90 min.

Fourth, DTI may be a promising imaging technique that evaluates the microstructure changes of WM tracts. The loss of the myelin is commonly related to an increase in the RD value, and axonal injury results in an increase in the AD value and MD value [8]. Although AD, RD and MD increased with decreasing DVR in our study, their correlation was week suggesting that $^{18}$F-florbetapir PET and DTI parameters are indeed measures with distinct specificities. In fact, multiple pathological factors affecting the diffusion of water in the WM tract, including demyelination, axon damage, microglia activation and gliosis, could lead to changes in DTI signals, so DTI detects the overall structure change of the WM tract, not just the changes in myelin [33, 34]. Furthermore, compared

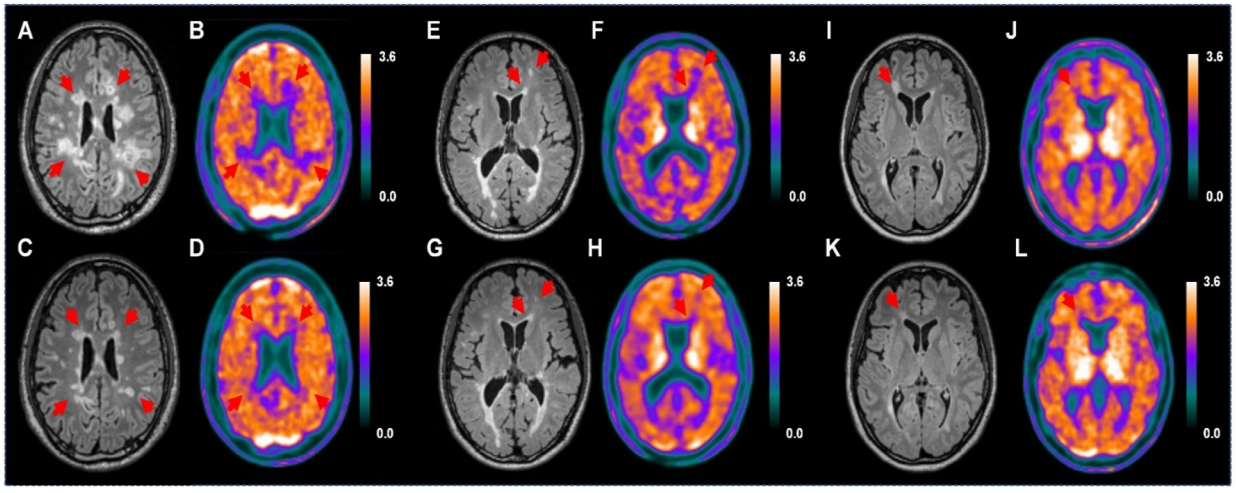


**Fig. 5.** (A-L) Longitudinal change from baseline to follow-up of representative DWM lesions on T2 FLAIR MRI and $^{18}$F-florbetapir DVR map (The top row of images was from the baseline scan, while the bottom row of images was from the follow-up scan) from the patients No. 23 (A-D), No. 5 (E-H) and No. 11 (I-L), respectively. Both focal areas of T2 hyperintensity (red arrow) and those of abnormally reduced $^{18}$F-florbetapir binding in DWM lesions decreased from baseline to follow-up, suggesting that myelin recovery might occur after inflammation disappearance. DVR: distribution volume ratio; DWM: damaged white matter; MRI: magnetic resonance imaging.

with the HCs, the patients with MS seemed to have lower FA and higher RD in the whole NAWM in our study. A previous study with a larger sample also showed that DTI-derived FA and RD could quantify NAWM damage in MS [8]. This change may be related to the presence of microdemyelination, which was supported by postmortem brain autopsy of patients with MS [35]. However, the binding level of $^{18}$F-florbetapir in the whole NAWM between patients with MS and HCs showed no difference in our study, which is similar to previous studies using $^{11}$C-PiB [12] and $^{18}$F-florbetapir [22], suggesting that the limitation of the $^{18}$F-florbetapir PET resolution may make it difficult to detect microdemyelination.

The number of patients in our longitudinal PET study was relatively limited. Therefore, as this is an exploratory study, more samples are needed to further assess the diagnostic performance of $^{18}$F-florbetapir PET in monitoring myelin loss and recovery. Additionally, lesions smaller than the resolution limit of our PET (4.2 mm) could not be evaluated in this study. In fact, these small lesions may still have an impact on the patient's clinical symptoms and disability. Additionally, due to a non-random and small sample in this observational study, data were presented only as descriptive results without statistically significant analysis, which will be carried out in our next study with random and larger samples.

In summary, with a longer half-life than $^{11}$C-PiB, $^{18}$F-florbetapir PET was a very promising tool for quantitatively monitoring myelin loss and recovery in patients with MS. Hybrid $^{18}$F-florbetapir PET/MRI could synchronously provide information on the myelin content change and microstructure change of WM tracts in DWM lesions and NAWM of patients with MS, and will become a powerful technique for evaluating the efficacy of remyelination-targeted drugs in the future.

## Funding

This research was supported by Shanghai Pujiang Program (18PJD030), Shanghai Municipal Key Clinical Specialty (shslczdzk03403), Shanghai Shuguang Plan Project (18SG15), Shanghai Health and Family Planning Commission Research Project (201840001), Clinical Research Plan of SHDC (SHDC2020CR2027B). FC and MZ are supported by the French Ministry of Foreign Affairs (French-Chinese program "Xu Guangqi", Project No. 45620ZE). The funding sources had no role during the study design; in the collection, analysis, or interpretation of data; in the writing of the report; or in the decision to submit the paper for publication.

## Authors' contributions

Conceptualization, Min Zhang, Biao Li and Sheng Chen; Data curation, Min Zhang; Formal analysis, You Ni, Qinming Zhou; Investigation, Lu He, Huanyu Meng, Yining Gao; Methodology, Xinyun Huang, Hongping Meng, Peihan Li, Meidi Chen, Danni Wang, Jingyi Hu, Qiu Huang, Yao Li; Project administration, Min Zhang and Biao Li; Supervision, Sheng Chen; Writing – original draft, Min Zhang; Writing - review & editing, Fabien Chauveau and Sheng Chen. All authors had full access to all of the data in the study and take responsibility for the accuracy of the data and the integrity of the data analysis.

## Data sharing statement

All the data used during the current study are included in the article and supplementary material. For further information on data sharing, please contact the corresponding author.

## Declaration of Competing Interest

The authors have declared that no competing interest exists.

## Acknowledgements

We thank Prof. Kung Hank F from University of Pennsylvania, Philadelphia, US and Prof. Lin Zhu from Beijing Normal University, Beijing, China for kindly supplying the florbetapir probe precursor for us and synthesis technical support. We thank Ph.D. Jian Li from clinical research center, Ruijin hospital, Shanghai Jiao Tong University School of Medicine, Shanghai, China for statistical analysis guidance.

## Supplementary materials

Supplementary material associated with this article can be found, in the online version, at doi:10.1016/j.eclinm.2021.100982.

## References

[1] Compston A, Coles A. Multiple sclerosis. Lancet 2002;359(9313):1221–31.
[2] Tian DC, Zhang CY, Yuan M, Yang X, Shi FD. Incidence of multiple sclerosis in China: a nationwide hospital-based study. Lancet Reg Health 2020;1:100010.
[3] D eshmukh VA, Tardif V, Lyssiotis CA, Green CC, Kerman B, Kim HJ, et al. A regenerative approach to the treatment of multiple sclerosis. Nature 2013;502(7471):327–32.
[4] Najm FJ, Madhavan M, Zaremba A, Shick E, Karl RT, Factor DC, et al. Drug-based modulation of endogenous stem cells promotes functional remyelination in vivo. Nature 2015;522(7555):216–20.
[5] Plemel JR, Liu WQ, Yong VW. Remyelination therapies: a new direction and challenge in multiple sclerosis. Nat Rev Drug Discov 2017;16(9):617–34.
[6] Cadavid D, Balcer L, Galetta S, Aktas O, Ziemssen T, Vanopdenbosch L, et al. Safety and efficacy of opicinumab in acute optic neuritis (RENEW): a randomised, placebo-controlled, phase 2 trial. Lancet Neurol 2017;16(3):189–99.
[7] Enzinger C, Barkhof F, Ciccarelli O, Filippi M, Kappos L, Rocca MA, et al. Nonconventional MRI and microstructural cerebral changes in multiple sclerosis. Nat Rev Neurol 2015;11(12):676–86.
[8] Roosendaal SD, Geurts JJ, Vrenken H, Hulst HE, Cover KS, Castelijns JA, et al. Regional DTI differences in multiple sclerosis patients. Neuroimage 2009;44(4):1397–403.
[9] Bouhrara M, Rejimon AC, Cortina LE, Khattar N, Bergeron CM, Ferrucci L, et al. Adult brain aging investigated using BMC-mcDESPOT-based myelin water fraction imaging. Neurobiol Aging 2020;85:131–9.
[10] Ercan E, Varma G, Madler B, Dimitrov IE, Pinho MC, Xi Y, et al. Microstructural correlates of 3D steady-state inhomogeneous magnetization transfer (ihMT) in the human brain white matter assessed by myelin water imaging and diffusion tensor imaging. Magn Reson Med 2018;80(6):2402–14.
[11] Stankoff B, Freeman L, Aigrot MS, Chardain A, Dolle F, Williams A, et al. Imaging central nervous system myelin by positron emission tomography in multiple sclerosis using [methyl-$^{11}$C]-2-(4′-methylaminophenyl)-6-hydroxybenzothiazole. Anna Neurol 2011;69(4):673–80.
[12] Bodini B, Veronese M, Garcia-Lorenzo D, Battaglini M, Poirion E, Chardain A, et al. Dynamic imaging of individual remyelination profiles in multiple sclerosis. Anna Neurol 2016;79(5):726–38.
[13] Veronese M, Bodini B, Garcia-Lorenzo D, Battaglini M, Bongarzone S, Comtat C, et al. Quantification of [(11)C]PIB PET for imaging myelin in the human brain: a test-retest reproducibility study in high-resolution research tomography. J Cerebr Blood F Met 2015;35(11):1771–82.
[14] Grecchi E, Veronese M, Bodini B, Garcia-Lorenzo D, Battaglini M, Stankoff B, et al. Multimodal partial volume correction: application to [(11)C]PIB PET/MRI myelin imaging in multiple sclerosis. J Cerebr Blood F Met 2017;37(12):3803–17.
[15] Bajaj A, LaPlante NE, Cotero VE, Fish KM, Bjerke RM, Siclovan T, et al. Identification of the protein target of myelin-binding ligands by immunohistochemistry and biochemical analyses. J Histochem Cytochem 2013;61(1):19–30.
[16] Glodzik L, Rusinek H, Li J, Zhou C, Tsui W, Mosconi L, et al. Reduced retention of Pittsburgh compound B in white matter lesions. Eur J Nucl Med Mol I 2015;42(1):97–102.
[17] Goodheart AE, Tamburo E, Minhas D, Aizenstein HJ, McDade E, Snitz BE, et al. Reduced binding of Pittsburgh compound-B in areas of white matter hyperintensities. NeuroImage-Clin 2015;9:479–83.
[18] Zeydan B, Lowe VJ, Schwarz CG, Przybelski SA, Tosakulwong N, Zuk SM, et al. Pittsburgh compound-B PET white matter imaging and cognitive function in late multiple sclerosis. Mult Scler 2018;24(6):739–49.
[19] Auvity S, Tonietto M, Caille F, Bodini B, Bottlaender M, Tournier N, et al. Repurposing radiotracers for myelin imaging: a study comparing 18F-florbetaben, 18F-florbetapir, 18F-flutemetamol,11C-MeDAS, and 11C-PiB. Eur J Nucl Med Mol I 2020;47(2):490–501.
[20] Zhang M, Liu J, Li B, Chen S. 18)F-florbetapir PET/MRI for quantitatively monitoring demyelination and remyelination in acute disseminated encephalomyelitis. EJNMMI Res 2019;9(1):96.
[21] Pietroboni AM, Carandini T, Colombi A, Mercurio M, Ghezzi L, Giulietti G, et al. Amyloid PET as a marker of normal-appearing white matter early dam-

age in multiple sclerosis: correlation with CSF beta-amyloid levels and brain volumes. Eur J Nucl Med Mol I 2019;46(2):280–7.
[22] Carotenuto A, Giordano B, Dervenoulas G, Wilson H, Veronese M, Chappell Z, et al. [(18)F]Florbetapir PET/MR imaging to assess demyelination in multiple sclerosis. E. Eur J Nucl Med Mol I 2020;47(2):366–78.
[23] Matías-Guiu JA, Cabrera-Martín MN, Matías-Guiu J, Oreja-Guevara C, Riola–Parada C, Moreno-Ramos T, et al. Amyloid PET imaging in multiple sclerosis: an (18)F-florbetaben study. BMC Neurol 2015;15:243 Nov 25.
[24] Pytel V, Matias-Guiu JA, Matías-Guiu J, Cortés-Martínez A, Montero P, Moreno-Ramos T, et al. Amyloid PET findings in multiple sclerosis are associated with cognitive decline at 18 months. Mult Scler Relat Disord 2020;39:101926 Jan 2.
[25] Thompson AJ, Banwell BL, Barkhof F, Carroll WM, Coetzee T, Comi G, et al. Diagnosis of multiple sclerosis: 2017 revisions of the McDonald criteria. Lancet Neurol 2018;17(2):162–73.
[26] Egger C, Opfer R, Wang C, Kepp T, Sormani MP, Spies L, et al. MRI FLAIR lesion segmentation in multiple sclerosis: does automated segmentation hold up with manual annotation? NeuroImage-Clin 2017;13:264–70.
[27] Logan J, Fowler JS, Volkow ND, Wang GJ, Ding YS, Alexoff DL. Distribution volume ratios without blood sampling from graphical analysis of PET data. J Cerebr Blood F Met 1996;16(5):834–40.
[28] De Groot CJ, Bergers E, Kamphorst W, Ravid R, Polman CH, Barkhof F, et al. Post-mortem MRI-guided sampling of multiple sclerosis brain lesions: increased yield of active demyelinating and (p) reactive lesions. Brain 2001;124(Pt 8):1635–45.
[29] van Walderveen MA, Kamphorst W, Scheltens P, van Waesberghe JH, Ravid R, Valk J, et al. Histopathologic correlate of hypointense lesions on T1-weighted spin-echo MRI in multiple sclerosis. Neurology 1998;50(5):1282–8.
[30] Datta G, Colasanti A, Rabiner EA, Gunn RN, Malik O, Ciccarelli O, et al. Neuroinflammation and its relationship to changes in brain volume and white matter lesions in multiple sclerosis. Brain 2017;140(11):2927–38.
[31] Brück W, Bitsch A, Kolenda H, Brück Y, Stiefel M, Lassmann H. Inflammatory central nervous system demyelination: correlation of magnetic resonance imaging findings with lesion pathology. Ann Neurol 1997;42(5):783–93 Nov.
[32] Duan Y, Liu Z, Liu Y, Huang J, Ren Z, Sun Z, et al. Metabolic changes in normal-appearing white matter in patients with neuromyelitis optica and multiple sclerosis: a comparative magnetic resonance spectroscopy study. Acta Radiol 2017;58(9):1132–7.
[33] Schmierer K, Wheeler-Kingshott CA, Boulby PA, Scaravilli F, Altmann DR, Barker GJ, et al. Diffusion tensor imaging of post mortem multiple sclerosis brain. Neuroimage 2007;35(2):467–77.
[34] Seewann A, Vrenken H, van der Valk P, Blezer EL, Knol DL, Castelijns JA, et al. Diffusely abnormal white matter in chronic multiple sclerosis: imaging and histopathologic analysis. Arch Neurol 2009;66(5):601–9.
[35] Kolasinski J, Stagg CJ, Chance SA, Deluca GC, Esiri MM, Chang EH, et al. A combined post-mortem magnetic resonance imaging and quantitative histological study of multiple sclerosis pathology. Brain 2012;135(Pt 10):2938–51.